J. Fluid Mech. (1981), *vol.* 109, *pp.* 367–389
Printed in Great Britain

Steady, supercritical flow in collapsible tubes. Part 1. Experimental observations

By IFIYENIA KECECIOGLU, MICHAEL E. McCLURKEN, ROGER D. KAMM AND ASCHER H. SHAPIRO

Fluid Mechanics Laboratory, Department of Mechanical Engineering, Massachusetts Institute of Technology, Cambridge, Massachusetts 02139, U.S.A.

(Received 19 May 1980 and in revised form 10 October 1980)

Experimental results are presented for steady, supercritical flow of a liquid in a thin-walled compliant tube which is in a state of partial collapse due to a negative transmural pressure. Particular attention is paid to the effects of longitudinal tension.

With a constant external pressure, friction acts to increase the area in the downstream direction. With the tube tilted downward, friction may be so balanced by gravity forces as to result in an asymptotic approach to an equilibrium situation in which the area and velocity remain constant. When the downstream pressure is increased sufficiently, shock-like transitions to subcritical inflated states, with positive transmural pressure, occur. The longitudinal length scale of the shock is on the order of one to several tube diameters. The pressure rise across the shock lies between that for loss-free pressure recovery and that given by the Borda–Carnot sudden-expansion theory.

The presence of longitudinal tension causes a train of standing waves of area to appear upstream of a local area disturbance, such as a shock-like transition. The standing waves are superimposed upon the more gradual area changes associated with friction and gravity. The wave amplitude grows in the downstream direction. Theoretical interpretations of the observations are presented in the companion paper (part 2).

1. Introduction

1.1. *Subject and scope*

This paper presents experimental results for steady, supercritical flows in a thin-walled, compliant tube, mounted under longitudinal tension, when the tube is partially collapsed by reason of a negative transmural (internal minus external)) pressure. 'Supercritical' here signifies that the mean flow velocity exceeds the longitudinal phase velocity, c_∞, of long waves of one-dimensional area variation. Theoretical interpretations of the observations are presented in a companion paper (McClurken *et al.* 1981), hereinafter referred to as part 2.

In the absence of longitudinal tension and longitudinal bending stiffness, continuous streamwise gradients in velocity and area are brought about by friction, gravity, gradients of external pressure, etc. (e.g. Shapiro 1977*a*). The thrust of the present paper and of part 2 is toward two other phenomena exhibited in the photographs of

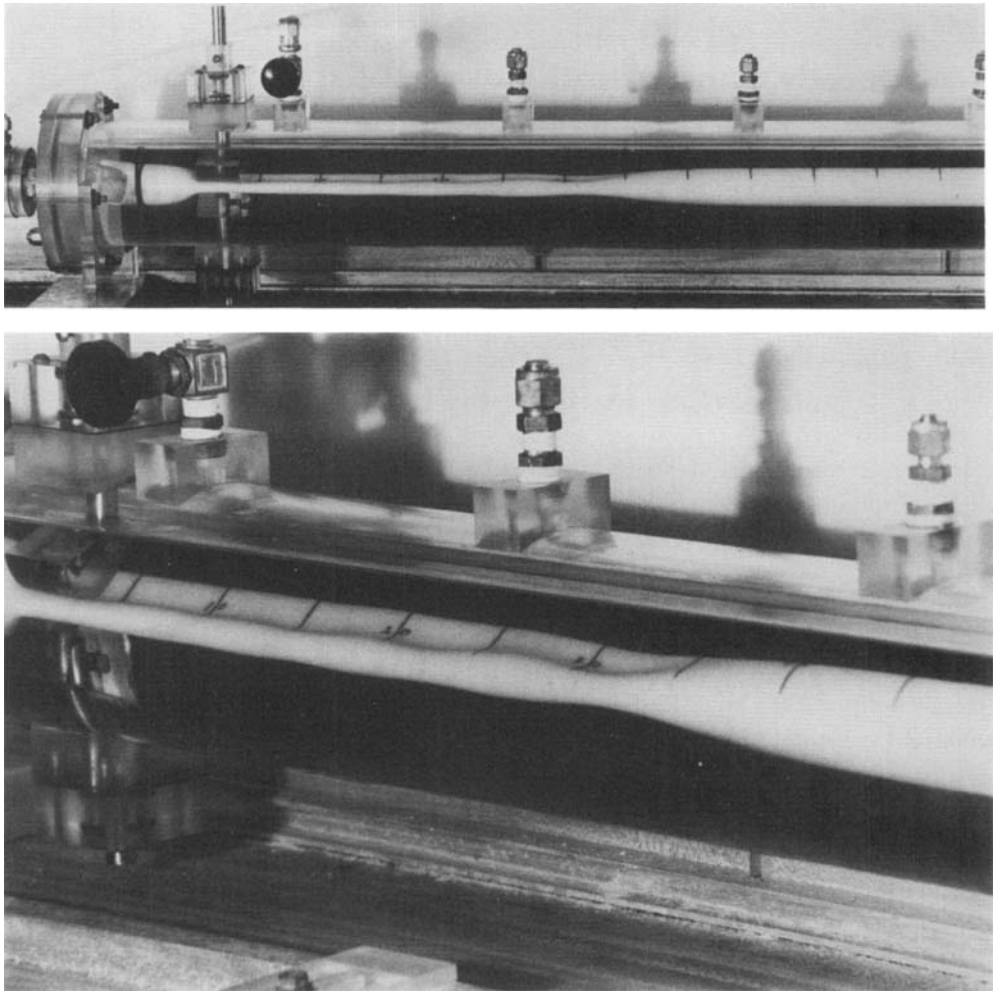

FIGURE 1. Photographs of apparatus, showing a standing shock wave and standing precursor waves due to tension. Flow is from left to right. (*a*) Long view; (*b*) close-up.

figure 1: (i) standing waves of area that occur by reason of stiffness due to longitudinal tension and to longitudinal bending, primarily the former; and (ii) shock-like transitions from supercritical, partially collapsed states to subcritical, inflated states.

1.2. *Significance of the problem*

Flows in collapsible tubes are of interest mainly in physiology and with respect to certain medical devices (e.g. Shapiro 1977*b*).

Physiological applications are to be found (i) in the circulatory system, principally on the venous side; (ii) in the pulmonary system, both in the airways and in the pulmonary circulation; (iii) in the urethra; (iv) possibly in the Eustachian tubes and in the drainage of aqueous humour from the eye; (v) relatedly, in functioning of the vocal cords; (vi) possibly in so-called 'autoregulation' of blood flow to systemic organs; and (vii) in a variety of sounds heard in the cardiovascular and pulmonary systems.

Among the clinical devices involving flow in collapsible tubes are (i) the occlusive

method of measuring blood pressure; (ii) pressurizing cuffs for diagnosing occlusive disease and thrombi in the limbs; (iii) intermittently pressurized boots or sleeves, installed on the lower extremities, employed as prophylaxis against deep-vein thrombosis in surgical patients; (iv) counterpulsation techniques (by the use of either an intra-aortic balloon or inflatable sleeves on the legs) under electrocardiogram command, as temporary but relatively non-invasive means of cardiac assist; and (v) certain forms of externally worn prosthetic larynxes.

1.3. *Previous work*

(*a*) *Studies based on a 'local tube law'.* Virtually all the literature on flow in collapsible tubes contains the assumption that there exists a 'local tube law', namely a unique relationship, $A = A(p-p_e)$, between the local cross-sectional area, A, and the local transmural pressure, $p-p_e$. This is valid when the stiffness against area change resides solely in circumferential bending or tension; or, equivalently, when the structural stiffnesses due to longitudinal tension and bending are both negligible. But such is the case only if longitudinal area variations are of sufficiently long wavelength. Thus the hypothesis of a local tube law is equivalent to the assumption of infinite wavelength in area variations.

The infinite-wavelength phase velocity, c_∞, for wave propagation in area-compliant vessels containing an incompressible fluid (Weber 1866) is

$$c_\infty^2 = \frac{A}{\rho}\frac{d(p-p_e)}{dA} = \frac{K_p}{\rho}\alpha\frac{d\mathscr{P}}{d\alpha}, \tag{1}$$

where ρ is the fluid density; A_0 is the value of A at zero transmural pressure, which may, however, be affected by longitudinal extension through Poisson's ratio; $\alpha \equiv A/A_0$. The circumferential bending stiffness, K_p, for a linear elastic material, is given by $K_p = \frac{1}{12}E(h/R_0)^3/(1-\nu^2)$, E is Young's modulus, ν is Poisson's ratio, h is the wall thickness, $R_0 \equiv \frac{1}{2}D_0$ is the radius of a circle of area A_0; and $\mathscr{P} \equiv (p-p_e)/K_p$. The quantities $\mathscr{P}$ and α are respectively the dimensionless transmural pressure and area.

Steady flows obeying a local tube law are somewhat analogous to one-dimensional gasdynamic and free-surface flows (Griffiths 1969, 1971*a*, *b*, 1973; Oates 1975; Shapiro 1977*a*), with $\mathscr{P}(\alpha)$ playing the role of the equation of state in gasdynamics. The speed index, $S \equiv u/c_\infty$, where u = mean fluid speed, is analogous to the Mach number and the Froude number. Supercritical ($S > 1$) and subcritical ($S < 1$) flows produce opposite effects. Thus, if $S < 1$, friction causes the area and pressure to decrease, while the opposite is so when $S > 1$. Notably, the sign of dS/dx depends not only upon the sign of $(1-S)$, but also upon whether the property of the local tube law defined by

$$\mathscr{M}(\alpha) \equiv 3 + \frac{\alpha d^2\mathscr{P}/d\alpha^2}{d\mathscr{P}/d\alpha} \tag{2}$$

is positive (e.g. friction causes S to increase in subcritical flow) or negative (e.g. friction causes S to decrease in subcritical flow).

(*b*) *Shock waves.* The formation of shock waves by nonlinear steepening of propagating finite-amplitude area waves depends upon the same property, $\mathscr{M}(\alpha)$ (Olsen & Shapiro 1967; Nicholson, Heiser & Olsen 1967; Oates 1975; Shapiro 1977*a*; Kamm & Shapiro 1979). When $\mathscr{M}(\alpha) > 0$, compression waves steepen; when $\mathscr{M}(\alpha) < 0$, rarefaction waves steepen.

Nonlinear analyses of steady flow in compliant tubes also indicate effects suggesting shock wave formation (Lambert 1958; Beam 1968; Rudinger 1970; Anliker, Rockwell & Ogden 1971; Kivity & Collins 1974). These studies are directed mainly toward inflated tubes (as in the arterial system) and thus do not involve the large area changes and more severe nonlinearities typical of shock-like structures when the tube is partially collapsed.

A simple experiment by Griffiths (1971*a*) provided clear visual evidence of a stationary shock-like transition with a large increase of area: upstream of the shock the tube was partially collapsed and (it is here presumed) the flow was supercritical, downstream the tube was inflated. More detailed experimental studies of shock-like transitions from supercritical, partially collapsed states to subcritical, inflated states were reported by Kececioglu, Kamm & Shapiro (1978), by Kececioglu (1979), and by Elliott & Dawson (1979). Oates (1975) and Shapiro (1977*a*) suggested what now appear to be overly simple analyses of such a shock transition.

(*c*) *Effects of longitudinal tension and bending.* Ahead of a stationary shock transition from a collapsed to an inflated state there may appear a train of stationary precursor waves (Kececioglu *et al.* 1978). These were shown by Kececioglu (1979) to be due to longitudinal tension. Such tension-induced waves are analogous to capillary waves on a free surface.

When fluid flows past a compliant panel, the system becomes unstable at sufficiently high flow velocities, resulting in either catastrophic collapse or flutter. The observed instabilities are partly due to the effects of longitudinal tension and bending. To predict the instability limit for a partially collapsed compliant tube, the rather complex cross-sectional shape has been more simply modelled as a two-dimensional channel with compliant walls (Weaver & Paidoussis 1977; Matsuzaki & Fung 1977) and as a biconcave channel (Raman 1967). The theoretical results exhibit both instability limits and wave speed dispersion. The particular dispersive properties of such waves in a compliant vessel makes it possible for standing waves to be superimposed upon a steady flow if the flow speed is greater than c_∞.

2. Experimental apparatus

2.1. *Overview of the measurements*

The goal of the experimental programme was to measure cross-sectional area and internal pressure as a function of axial distance for steady flows with a variety of supercritical inlet conditions and downstream pressures.

Because the tubes used were thin-walled and highly compliant, most of the conventional techniques of experimental fluid mechanics are impractical. The very difficult problem of measurement was largely solved through development of an electric impedance technique by means of which the local cross-sectional area could be measured without knowledge of the specific cross-sectional shape.

Using this technique, the local tube law $\mathscr{P}(\alpha)$ of a particular tube was first determined under conditions of zero flow and zero longitudinal tension. Then, using equation (1), $c_\infty(\alpha)$ was inferred from the smoothed data for $\mathscr{P}(\alpha)$. Subsequently, in a flow experiment, the flow rate and local cross-sectional area were measured, from which the area ratio α, the one-dimensional speed u, and the speed index $S \equiv u/c_\infty$ were calculated.

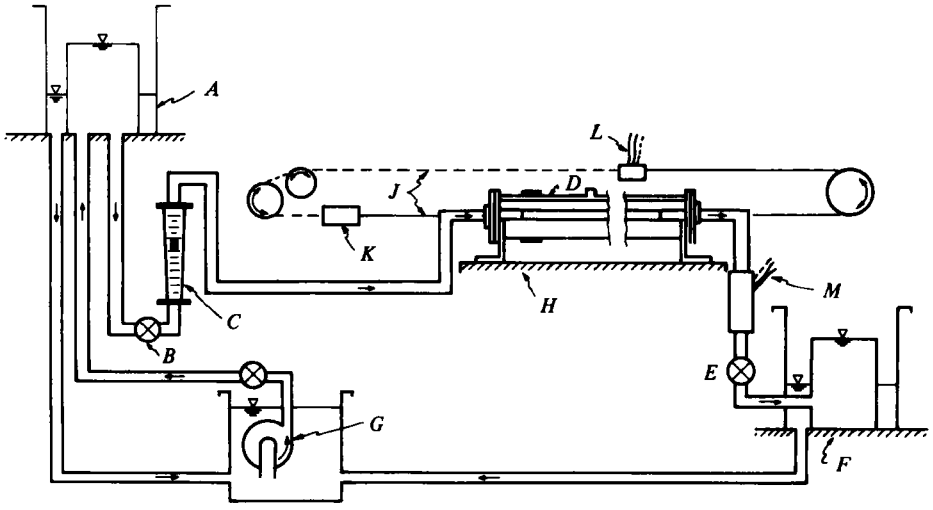

FIGURE 2. Schematic diagram of flow circuit. *A*, upstream head tank. *B*, valve for adjusting flow rate. *C*, flowmeter. *D*, test section. *E*, valve for adjusting downstream pressure. *F*, downstream head tank. *G*, pump. *H*, base. *J*, catheter traversing loop. *K*, pressure transducer. *L*, voltage leads for ΔV_l. *M*, voltage leads for ΔV_e.

2.2. *Flow circuit*

The working fluid, consisting of a 7 %-by-weight solution of sodium chloride in water, flowed from an upstream constant-head tank, through a flow-adjusting valve and a flowmeter, into the test section (see figure 2). From the test section the solution passed through a second valve, used mainly for controlling downstream pressure, and into a downstream constant-head tank, from which it was pumped back to the upstream tank.

(*a*) *Horizontal test section for tension–friction flows.* As seen in figures 1, 2 and 3, a tube of latex rubber (inside diameter 2·54 cm, wall thickness 0·086 cm, length 110 cm) was mounted on rigid cylindrical tubes that passed through the end caps of a flanged, clear Plexiglas test section (inside diameter 10·16 cm, length 130 cm). The latter was nearly filled with a glycerine–water mixture, adjusted to specific gravity 1·05, to negate the effects of gravity. A large tank, not shown, was connected directly to the air space in the Plexiglas test section above the glycerine–water surface; appropriately pressurized, this tank provided a stable, sensitive source of external pressure acting uniformly on the highly compliant latex tube through which flowed the working fluid.

The latex tube was fastened by means of O-rings to the rigid end tubes (inside diameter 2·22 cm, outside diameter 2·54 cm), which had been tapered to feathered edges in order to avoid area discontinuities. The O-ring seals between the rigid tubes and the Plexiglas test section allowed for both twist and axial motion, the former to assure a uniform plane of collapse, the latter for adjusting the longitudinal tension. The longitudinal strain was determined by measuring the distance between lines inked on the latex tube.

Supercritical flow was established by means of an adjustable sphincter nozzle which compresses the latex tube symmetrically in its twin-lobed mode. The rising–falling distribution of external pressure produced by the 'fingers' of the sphincter established

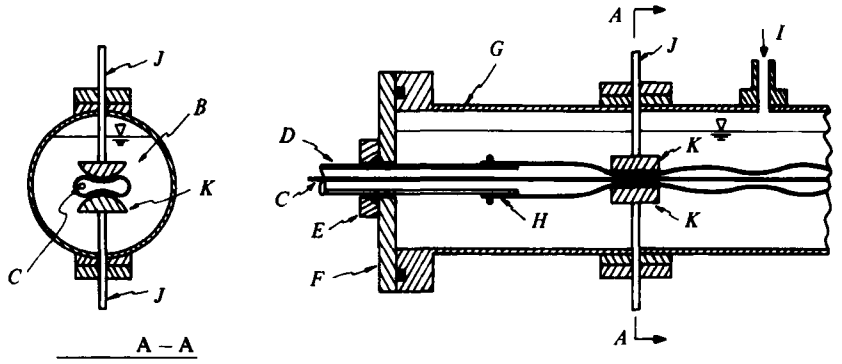

FIGURE 3. Detail of horizontal test section at inlet end, for tension–friction flows. *B*, glycerine–water mixture. *C*, catheter. *D*, rigid end tube. *E*, seal. *F*, end cap. *G*, Plexiglas test section. *H*, latex tube. *I*, source of external air pressure. *J*, rods for adjusting sphincter. *K*, fingers of sphincter.

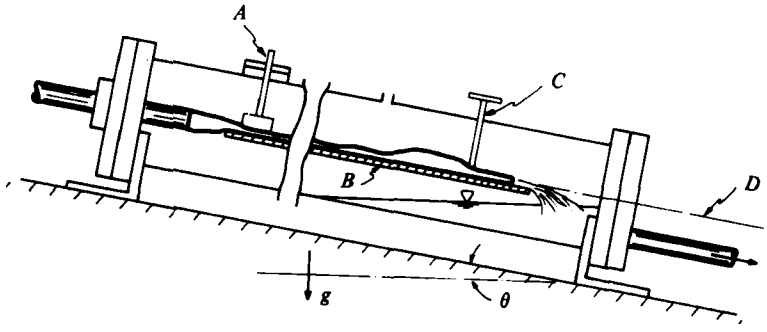

FIGURE 4. Arrangement of test section for gravity–friction flows. *A*, adjustment of sphincter nozzle. *B*, sloping support. *C*, source of disturbance near downstream end. *D*, catheter probe.

a subcritical-to-supercritical transition (Shapiro 1977*a*), analogous to the supersonic flow produced by a convergent–divergent nozzle in a supersonic wind tunnel. The setting of the sphincter constriction also established the area at the inlet to the supercritical flow region under test.

(*b*) *Sloping test section for gravity–friction flows.* For certain tests the test section was modified as shown in figure 4. The downstream rigid support and the gravity-cancelling glycerine–water mixture were removed. The tube was supported by a flat plate, with the downstream end left free. Without the buoyancy of the external liquid, the downward slope θ of the test section produced a streamwise component of gravity, $g \sin \theta$, acting on the working fluid.

With this arrangement the cross-sectional shape of the tube was no longer symmetrical about a horizontal axis. However, two countervailing benefits were gained: (i) disturbances associated with the adjustment of the latex tube to the area of the downstream rigid tube were eliminated; and (ii) streamwise frictional effects could, as it were, be cancelled by gravity, so that we could perform experiments effectively free of mean frictional effects.

(*c*) *Traversing catheter.* Longitudinal distributions of internal pressure and area were obtained by means of a closed-loop traversing catheter. The loop was formed from a length of hollow Teflon tubing (outside diameter 0·275 cm, inside diameter 0·180 cm)

attached to a length of fibre-reinforced-plastic sprocket chain. A constant-speed motor provided a stable drive for the loop.

The static pressure, sensed at a side hole in the Teflon tube, was transmitted through a length of stainless steel needle tubing (inside diameter 0·120 cm, outside diameter 0·165 cm) to a pressure transducer mounted on that part of the loop external to the test section. Just downstream of the static tap, the electrode-pair used for area measurement was epoxy-bonded into the Teflon tubing; the leads were run inside the tubing to a voltage pick-off further around the loop.

The catheter was positioned against the walls of the rigid tubes. Interference of the catheter with tube collapse did not occur until the area ratio α was below about 0·15.

The fluid velocity was calculated as $u = Q/(A - A_p)$, where A_p is the cross-sectional area of the catheter, and A the total cross-sectional area, including the catheter. The wave speed c_∞ was based on equation (1) at the value $\alpha \equiv A/A_0$; this procedure neglects the factor $[1 - (A_p/A)]^{\frac{1}{2}}$, which, however, never differed from unity by more than 2 %.

2.3. *Measurement of pressure*

(*a*) *Static conditions.* In order to determine the local tube law, internal and external pressures were measured under no-flow conditions. Simple single-column manometers were used for both the salt solution and the glycerine–water mixture.

The latex tube used for the experiments was extremely compliant in collapse: transition from a circular configuration to one with opposite walls in initial contact required a change in transmural pressure of less than 2 cm of water. Accordingly, the heights of the liquid columns were read using a cathetometer with a resolution of $\pm$ 0·005 cm water.

(*b*) *Flow conditions.* Under steady flow conditions, the traversing system previously described was employed, using a Gould Statham P23 unbonded strain-gauge type physiologic transducer. With the latter coupled to the stainless steel needle tubing, the system had a time constant of less than 50 ms as determined by test with a bursting balloon. This time response gave adequate spatial resolution with a traversing speed of 5 cm s^{-1}. However, to achieve this, it was necessary to use a transducer which had a full-scale range much larger than the levels of transmural pressure to be measured. Thus it was not always possible to obtain good noise-free output. This compromise was not seriously disadvantageous inasmuch as the area measurements provided the bulk of important data in steady flow. The static pressure data were used mainly to measure pressure recovery coefficients through standing shocks and to observe the phase of the changes in transmural pressure associated with standing tension waves. For these purposes the system was adequate.

2.4. *Area measurement by an electrical impedance technique*

The area-measurement technique developed for this investigation is a basic instrument for flow studies in collapsible tubes.

(*a*) *Principle of operation.* If the rate of change of area with respect to distance is sufficiently small, the resistance R of a short length L of non-uniform conductor may be approximated as $R = \rho L/A$, where ρ is the resistivity of the medium and A the cross-sectional area. The electrical impedance method is based on treating each length segment of conductive fluid inside the collapsible tube as a nearly cylindrical conductor of unknown area, in which the current flux is quasi-one-dimensional.

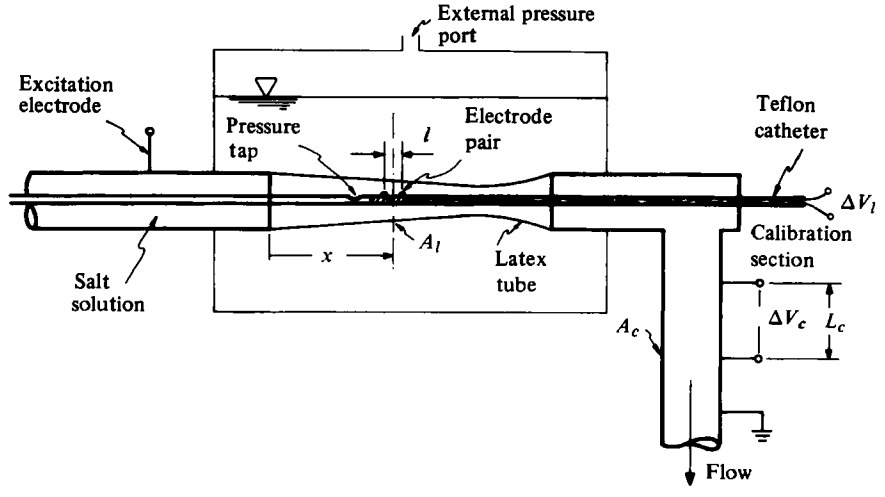

FIGURE 5. Electric impedance method for measuring cross-sectional area.

Three electrode pairs were used (figure 5). The first pair provided an a.c. voltage excitation from an electrode on the upstream rigid tubing to ground at the downstream rigid tubing, and established an a.c. current flow through the system. The second and third were sensing pairs coupled directly to high-impedance differential amplifiers having a high common-mode rejection ratio. The differential voltage ΔV_c was sensed at the calibration section, of length $L_c \cong 15$ cm and known cross-sectional area A_c. The differential voltage ΔV_l was sensed by an electrode pair, about 1 cm apart, epoxy-bonded into the Teflon catheter, at the location where the unknown cross-sectional area was to be measured.

The conductivities of the external glycerine–water solution and of the latex tube were so low relative to that of the salt solution inside the latex tube that current leakage was negligibly small. The two voltage-sensing pairs thus detected voltage drops across resistors arranged in series. The assumption that the current flux was one-dimensional leads to the formula

$$A_l = \frac{l}{L_c}\frac{\Delta V_c}{\Delta V_l}, \quad A_c = \text{constant} \times \frac{\Delta V_c}{\Delta V_l}, \tag{3}$$

where A_l is the unoccluded cross-sectional area. The total cross-sectional area A was found by adding to A_l the cross-sectional area A_p of the catheter.

(*b*) *Circuitry.* An analog circuit (figure 6) designed to implement equation (3) provided a continuous output voltage proportional to the unoccluded area A_l. The two sensing electrode pairs were direct coupled to high-quality differential amplifiers. In order to maintain a common-mode rejection ratio of over 100 dB, we did not use capacitive coupling at the input as a means of rejecting d.c. electrode potentials; instead, the d.c. offsets were amplified and rejected at the output. The two a.c. signals were sampled and held once per cycle, using synchronous pulses derived from the excitation voltage, and were then fed to the analog divider.

According to equation (3), the output of the divider is directly proportional to A_l. The constant of proportionality, including the gains of the differential amplifiers, was found simply by making a measurement with the catheter electrode pair located in one of the rigid tubes of known area.

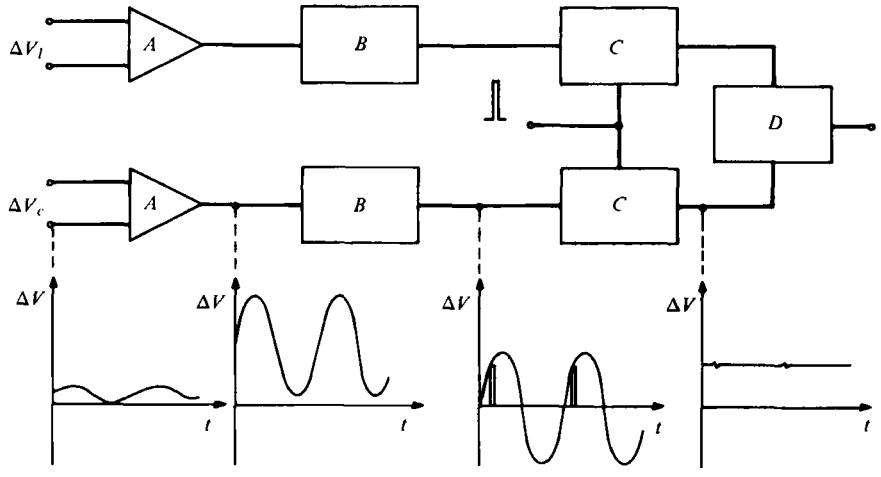

FIGURE 6. Analog circuit for producing output voltage proportional to area. *A*, differential amplifier. *B*, high-pass filter. *C*, sample-and-hold. *D*, divider.

(*c*) *Sources of error.* Several aspects of the technique, if not properly attended to, may produce unacceptably large errors. The most important of these arises from the non-ideal behaviour of differential amplifiers. Since the voltage drop across the catheter electrode pair is often as small as several millivolts with a common mode voltage of up to 5 volts, the amplifier must have a common-mode rejection ratio of at least 100 dB. If it does not, some fraction of the common mode appears at the output and affects the voltage ΔV_l. Also, since the rejection ratio decreases as frequency increases, the excitation frequency was kept as low as possible, typically around 200–500 Hz. Common mode errors were easily observed as falsely low area output when the probe was nearest the upstream excitation electrode.

If the liquid external to the latex tube has the same resistivity as the salt solution, a falsely high area is inferred owing to current leaking resistively through the latex tube and through the external current path. This predicament was avoided by using the glycerine–water mixture, the resistivity of which is about 10^4 times greater than that of the salt solution.

In order to verify that the technique is not unduly sensitive to large gradients in area or changes in shape, a converging–diverging section of 2·54 cm outside-diameter rigid Plexiglas tubing was formed with a heat gun. A reduction in area to 38 % of circular, over a distance of two diameters, was thereby produced, approximating the shock geometries discussed later. The area inferred using the electrical impedance method agreed within about $\pm$ 2 % with the area determined by direct volume measurement (McClurken 1978). Another check using a rigid uniform tube with a slowly tapering cylindrical insert verified that small changes in area on the order of 1 % of the circular area could be resolved easily.

3. Experimental results

3.1. *The local tube law*

The function $\mathscr{P}(\alpha)$ was determined by mounting the tube with zero axial strain and, at a location far from the ends, simultaneously measuring the cross-sectional area (by the electrical impedance method) and transmural pressure (with manometers) as liquid was slowly withdrawn from the interior. Since the unstressed tube was not perfectly round, the area A_0 corresponding to zero transmural pressure was also obtained by electric impedance measurement, rather than from geometric measurement.

In the range $\alpha \leqslant 0{\cdot}21$, for which the theory (Flaherty, Keller & Rubinow 1972) states that line contact prevails in a thin-walled tube, the data fitted very well the theoretical $\frac{3}{2}$-power similarity law; except, however, that for $\alpha < 0{\cdot}15$ the probe interfered with the tube wall and thus with the $\frac{3}{2}$-power relationship.

For calculating the dimensionless transmural pressure $\mathscr{P}$, the bending stiffness constant K_p was inferred from the pressure–area data in the similarity range, rather than from separate measurements of E, ν, h and R_0, which would have been less accurate. An *effective* value of K_p was inferred from the best fit of the data, in the range $0{\cdot}15 \leqslant \alpha \leqslant 0{\cdot}21$, to the $\frac{3}{2}$-power similarity law, here expressed in the form

$$\mathscr{P} = -1{\cdot}000\alpha^{-\frac{3}{2}} \tag{4}$$

where the proportionality constant has been given the value of exactly unity, instead of the theoretical value, namely 0·995.

(*a*) *The data for* $\mathscr{P}(\alpha)$. Figure 7 shows the experimental results expressed in the dimensionless form $\mathscr{P}(\alpha)$.

According to Tadjbakhsh & Odeh (1967), a tube initially circular buckles to an oval mode at $\mathscr{P}_B = -3$. Owing to the lack of perfect circularity the shape of the experimental curve of $\mathscr{P}(\alpha)$ near $\alpha = 1$ does not exhibit the sharp change in slope predicted by the theory. Nevertheless, $\mathscr{P}_B = -3$ is seen to be quite reasonable for the value at which the slope of $\mathscr{P}(\alpha)$ changes rapidly from a small value to a large value.

The sharp change in slope at $\alpha = 0{\cdot}27$ agrees well with the theoretical predictions of Flaherty *et al.*, according to which point contact starts at that area ratio, and there is a large concomitant change in slope.

(*b*) *The curve* $c_\infty(\alpha)$. Graphical smoothing and differentiation of the $\mathscr{P}(\alpha)$ data according to equation (1) produced the curve of $c_\infty(\alpha)$ also shown in figure 7. Several features are noteworthy. (*a*) The tube is relatively stiff in the range where opposite walls are in contact. (*b*) A local peak in c_∞ occurs between point and line contact. (*c*) In the range $0{\cdot}3 < \alpha < 0{\cdot}8$, the tube is very compliant: c_∞ is relatively small and is in fact nearly constant. (*d*) As the tube approaches roundness, it becomes relatively stiff again, the rapid increase in c_∞ occurring at about the theoretical buckling value, $\mathscr{P} \cong -3$.

(*c*) *Effect of longitudinal tension.* Only a single latex tube was used for all the experiments reported here, but it was stretched to different axial strains. Axial tension modifies both the area A_0 and the wall thickness. With any particular longitudinal strain, the corresponding value of A_0 was measured directly by means of the electric impedance method. If Poisson's ratio is the same in all directions, axial strain decreases both the circumference and the wall thickness by the same percentage. Hence K_p,

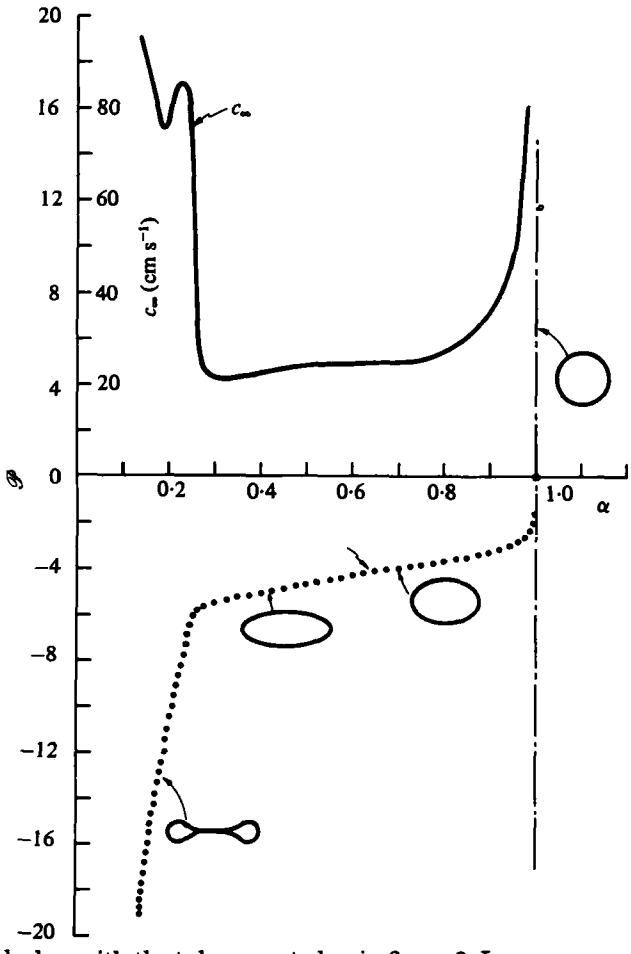

FIGURE 7. Local tube law with the tube mounted as in figure 3. Lower curve: experimental data of $\mathscr{P}(\alpha)$. Upper curve: $c_\infty(\alpha)$ from smoothed curve of $\mathscr{P}(\alpha)$.

which depends only upon the ratio of wall thickness to circumference, retains the value measured with no axial tension present.

(*d*) *Effect of a normal hydrostatic gradient.* With the arrangement of figure 4, the transmural pressure was no longer uniform around the perimeter. The tube sagged due to gravity and the shape lost its horizontal plane of symmetry.

For this case the local tube law was experimentally determined with the plane of the support taken as the datum level for pressure. Using the same values of A_0 and K_p obtained previously from the data of figure 7 for the gravity-free case, the curves for $\mathscr{P}(\alpha)$ and $c_\infty(\alpha)$ shown in figure 8 were determined.

Disregarding the arbitrary nature of the zero pressure datum, comparison of the $c_\infty(\alpha)$ curves in figure 7 and 8 reveals that the tube supported on a flat plate is stiffer in the range of intermediate area ratios, say $0{\cdot}3 < \alpha < 0{\cdot}7$. The relatively rapid area buckling in the vicinity of $\alpha = 1$ is missing from figure 8, and the point of touch contact appears to be delayed to about $\alpha \cong 0{\cdot}22$.

Although the tube properties are somewhat different for figures 7 and 8, their general

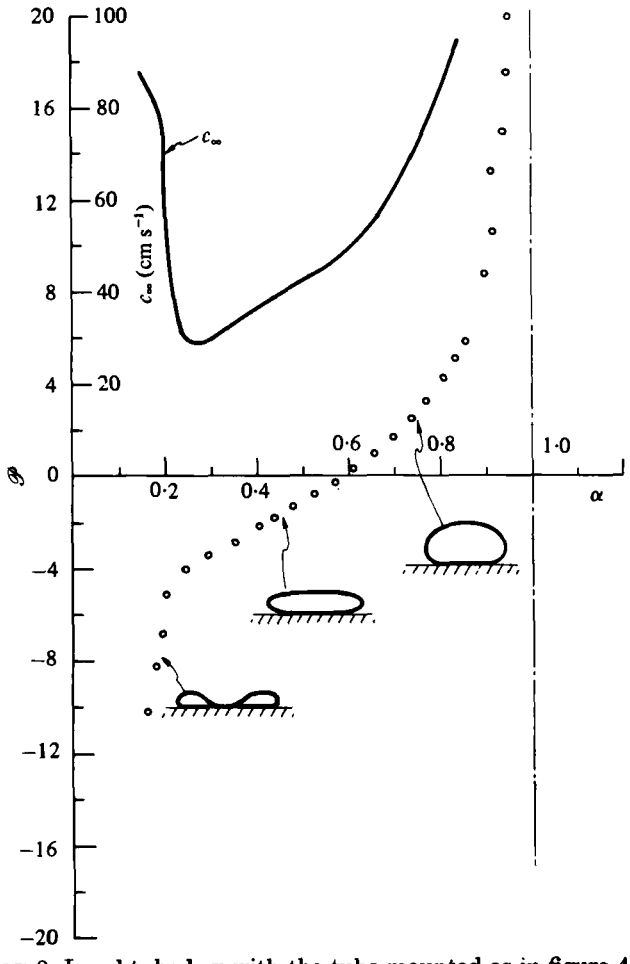

FIGURE 8. Local tube law with the tube mounted as in figure 4.

character remains the same, and the numerical values remain of the same order of magnitude. Consequently the qualitative features of flow behaviour should be essentially the same for the two different flow arrangements.

3.2. *Steady, supercritical flows*

(*a*) *Gravity–friction flows.* The tube mounting of figure 4 has two important consequences. First, axial tension is zero at the downstream free end. Further upstream, owing to skin friction, the axial tension is finite but it is very small (strain less than 1 %). Second, the absence of a rigid support at the downstream end eliminates several artifacts due to the constraint of connection to a rigid tube and, moreover, makes it easy to maintain the flow supercritical all the way to the exit.

The types of flow patterns that may occur depend, according to the one-dimensional theory, upon whether the flow is subcritical or supercritical, as well as upon a parameter expressing the ratio of gravity to friction forces (Shapiro 1977*a*), namely $\alpha^2\rho(g\sin\theta)\,D_0/K_pf$, where f is the skin-friction coefficient. With a supercritical inlet

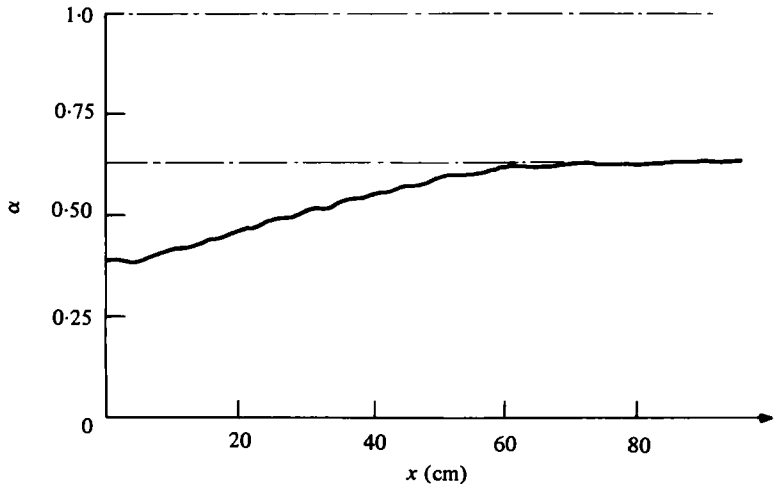

FIGURE 9. Supercritical gravity–friction flow. Slope, $\theta = 4{\cdot}8°$. Inlet conditions: $\alpha_1 = 0{\cdot}384$, $S_1 = 4{\cdot}2$. Asymptotic conditions: $\alpha_\infty = 0{\cdot}625$, $S_\infty = 1{\cdot}8$.

state, a sufficiently large value of this gravity-to-friction parameter produces a fluid acceleration (or deceleration), asymptotically toward a condition of unchanging area. At the asymptotic equilibrium condition the local gravity force just balances the local frictional force. With relatively large friction, the gravity–friction parameter is small, and the speed index S goes toward unity. At $S = 1$ the flow is choked and the solution cannot be continued; in practice, a standing shock transition usually intervenes.

These behaviour patterns are analogous to those which occur when a supercritical free-surface flow downstream of a sluice gate (i.e. the sphincter) passes down a constant-slope spillway. The analogy goes further. In a free-surface flow, the dispersion relationship is such that waves due to surface tension may stand ahead of a hydraulic jump. Similarly, it will be seen here and in part 2 that, in a supercritical collapsible-tube flow, even a small amount of longitudinal tension or bending establishes standing waves ahead of a source of disturbance.

(i) *Supercritical flow without shocks.* Figure 9 is an example of a flow without shocks. Within the latex tube, the curve of $\alpha(x)$ increases toward an equilibrium value at which friction is exactly balanced by gravity. The speed index, everywhere supercritical, decreases to an equilibrium value.

(ii) *Standing tension waves on a supercritical, uniform stream.* By suitable adjustment of the flow rate and sphincter setting, a supercritical flow was established in which the asymptotic equilibrium condition was reached very quickly (figure 10). Then, when the downstream end of the tube was disturbed in area by lightly touching a rod to the upper side of the tube, a train of standing waves was produced, with the amplitude attenuating in the upstream direction. This experiment gave clear evidence that the standing waves were the result of wave propagation upstream, against the flow.

(iii) *Standing shock waves.* When the disturbance due to the rod was made sufficiently large, a large-amplitude standing shock wave was produced (figure 11), which inflated the tube to $\alpha = 1$. The shock served as the source of a long train of attenuating tension waves which radiated upstream and stood stationary against the mean supercritical flow.

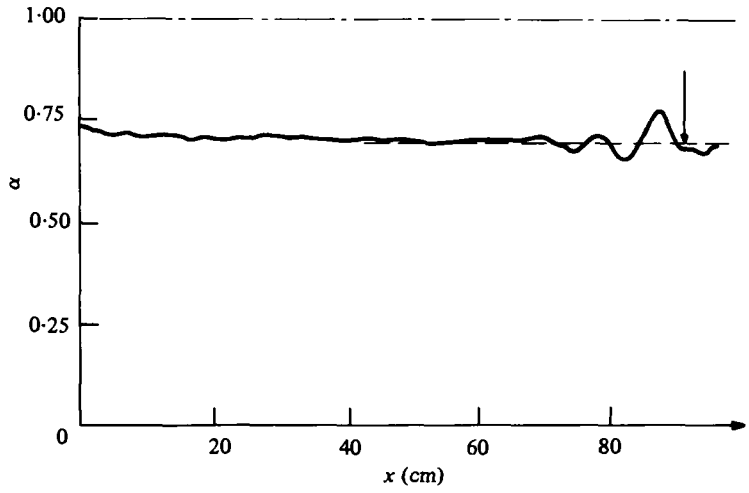

FIGURE 10. Supercritical gravity–friction flow with a rapid approach to an equilibrium state and a small source of disturbance (arrow) near exit. Slope, $\theta = 4{\cdot}8°$. Asymptotic conditions: $\alpha_\infty = 0{\cdot}70, S_\infty = 1{\cdot}40$.

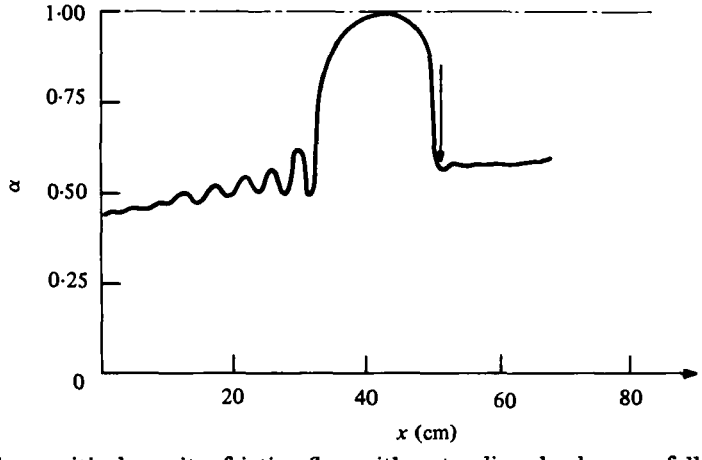

FIGURE 11. Supercritical gravity–friction flow with a standing shock wave, followed by a second supercritical region downstream of a second sphincter (arrow). Slope, $\theta = 9{\cdot}0°$. Inlet conditions: $\alpha_1 = 0{\cdot}45, S_1 = 4{\cdot}7$.

Downstream of the rod, the flow was again supercritical, demonstrating that the rod was serving as a second sphincter nozzle.

(*b*) *Tension–friction flows.* Using the test section of figure 3, longitudinal distributions of internal pressure and cross-sectional area were measured for flows with systematic variations of the parameters. The axial strain was varied from 0·023 to 0·174; the inlet speed index (just downstream of the sphincter) was varied from 1·5 to 10·4; the inlet area ratio was varied from 0·25 to 0·45; and the downstream pressure was varied to establish a standing shock at different distances from the sphincter.

(i) *Typical data record.* Figure 12 shows schematically the features of a typical data record in terms of the longitudinal distributions of unoccluded area, $A - A_p$, and of static pressure. Distinctly different segments of the area trace are to be seen, as identified in the caption to the figure.

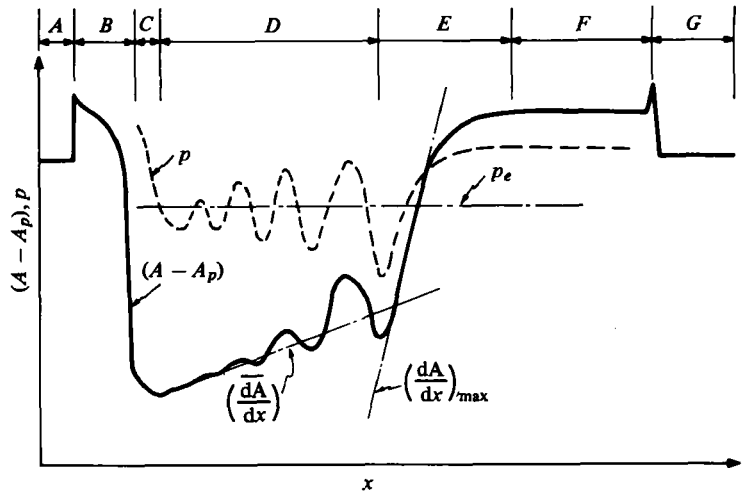

FIGURE 12. Typical data record for a tension–friction flow, with $\epsilon_x = 0{\cdot}11, \alpha_1 = 0{\cdot}276, S_1 = 10{\cdot}3$. *A*, upstream rigid tube. *B*, latex tube (inflated). *C*, sphincter. *D*, supercritical region (collapsed). *E*, shock transition. *F*, subcritical region (inflated). *G*, downstream rigid tube.

Downstream of the sphincter is a zone of supercritical flow in which there is a *mean* rate of area increase, $\overline{dA/dx}$, produced by friction. This is followed by a rapid area increase in a shock-like transition, at the exit of which the flow is subcritical with the tube inflated. The width of the shock is related to the value of the maximum gradient, $(dA/dx)_{max}$.

Superposed upon the mean area increase in the supercritical region is a train of tension-induced waves which appear to amplify in the downstream direction but which are better thought of as attenuating in the direction upstream of the shock, since it is the latter from which the waves are radiated.

The pressure record shows clearly the tension waves and the pressure rise through the shock, but not a mean pressure rise due to friction, corresponding to the mean area increase. This is explained as follows. The mean pressure rise (which is more or less independent of tension) is associated with area changes according to the local tube law. Inspection of figure 7 shows that in the mid-range of α, say $\alpha \cong 0{\cdot}5$, large changes of α involve only small changes in pressure. Typically, a change of α from 0·3 to 0·7 corresponds to a change in p of only 0·4 mmHg, which is too small to be measured by the transducer with a full-scale range of 200 mmHg.

For the standing waves, on the other hand, the pressure and area are related by longitudinal tension effects. More particularly, as shown in part 2, the oscillatory component of pressure is approximately proportional to $-T\,d^2A/dx^2$, where T is the tension force per unit perimeter. The magnitudes implied by this relationship are such that the spatial pressure *oscillations* are easily observed notwithstanding the relative insensitivity of the transducer. The data show that the pressure and area waves are in phase, as required by the relationship above.

(ii) *Adjustment of shock location.* Having set a particular value of axial strain without flow, the desired values of inlet area ratio and inlet speed index were established by adjustment of the sphincter and the upstream valve. Then the downstream pressure was reduced by opening the downstream valve until the longest possible run of

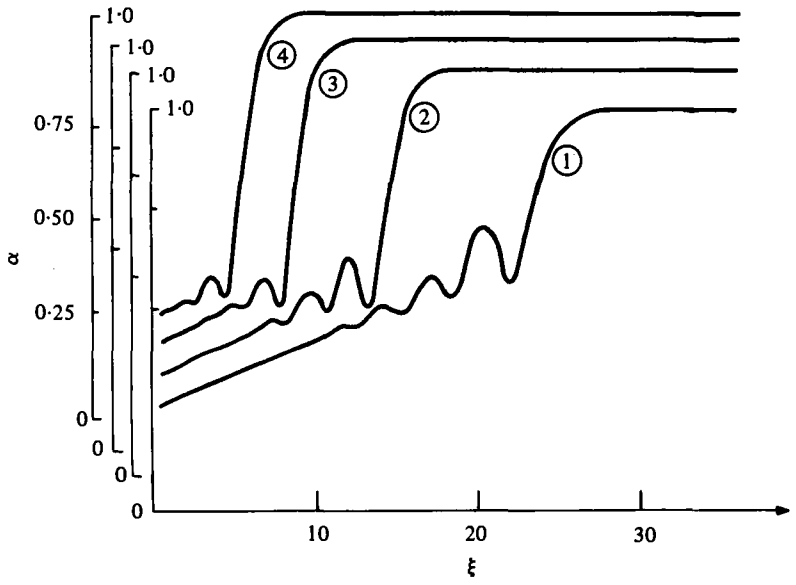

FIGURE 13. Effect of raising downstream pressure on shock location, for the conditions $\epsilon_x = 0{\cdot}023$, $\alpha_1 = 0{\cdot}27$, $S_1 = 8{\cdot}0$. Curves 1, 2, 3, 4 are for successively higher downstream pressures.

super-critical flow was obtained. Curve 1 of figure 13 shows $\alpha(\xi)$ for such a condition, where $\xi \equiv x/D_0$ is the normalized longitudinal co-ordinate. The shock was then moved to successive upstream positions, indicated by curves 2, 3, and 4, by gradual closure of the downstream valve.

As the shock moved upstream, the flow rate, the initial speed index, and that portion of the mean curve of $\alpha(\xi)$ upstream of the shock, all remained unaltered. This is a consequence of the mean flow being supercritical upstream of the shock, and therefore wholly independent of downstream conditions. The shock steepened as it moved upstream. Although the tension waves radiated by the shock changed in amplitude, the wavelength at a particular location remained constant.

(iii) *Categories of behaviour.* About 70 experimental runs were made. Many of the significant results extracted from the data, e.g. mean friction coefficients, wavelengths in relationship to flow speed and area ratio, attenuation coefficients for the waves, and shock widths, are presented in part 2 in comparison with the predictions of theoretical analysis. Here we present examples of the different types of phenomena observed, together with a largely empirical correlation of pressure recovery data across the shock.

For inlet area ratios typically about $\alpha \cong 0{\cdot}30$ the controlling parameters are the inlet speed index S_1 and the axial strain ϵ_x. By choosing various combinations of these, as well as the shock location, several categories of behaviour may be identified. Examples are shown in figure 14.

With small tension and small S_1 (figure 14*a*), the shock is weak and appears more like a large wave that is subcritical at its peak in area. With the same small tension but large S_1 (figure 14*b*), the wavelengths are shorter and the shock is shorter and better delineated, producing a subcritical, inflated state downstream.

With large tension, and a relatively low downstream pressure (figure 14*c*), friction

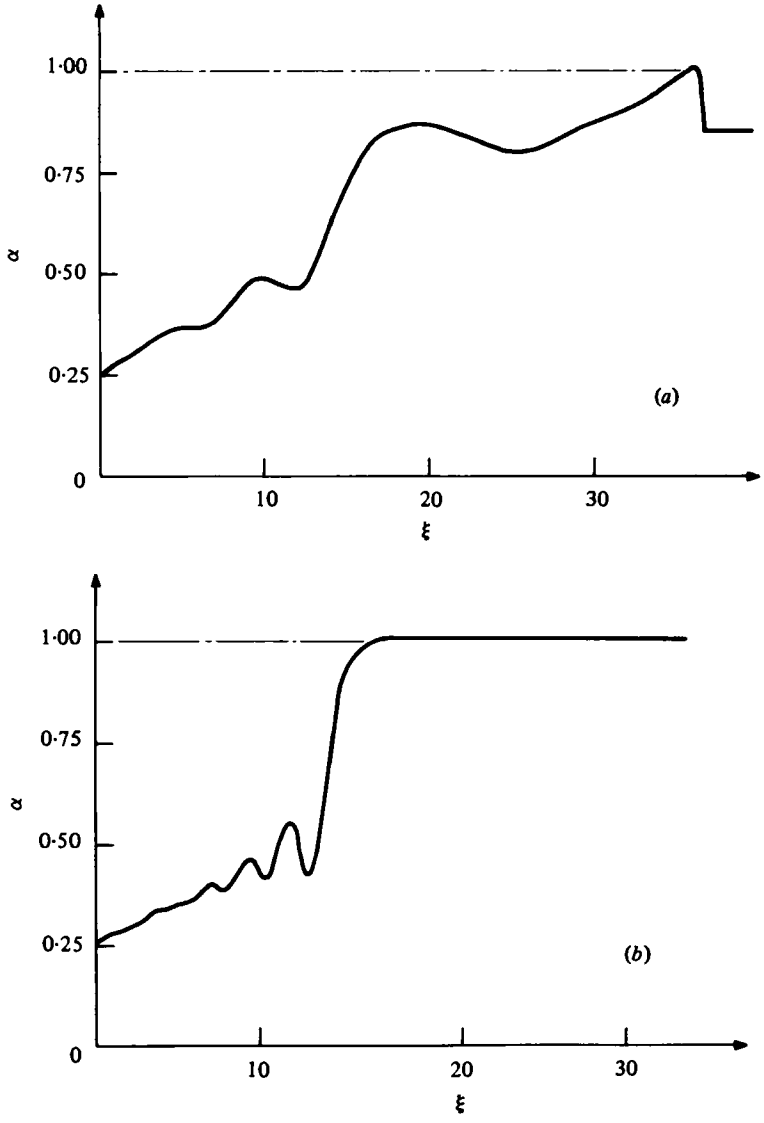

FIGURE 14(*a*, *b*). For the caption see next page.

produces a continuous, nearly linear increase of area. No shock is present, and standing waves, if any, are too weak to observe. With both large tension and large S_1, and with a sufficiently high downstream pressure (figure 14*d*), a rather broad shock appears, and with it a standing train of tension waves of large wavelengths. A comparison of figure 14(*a*) with 14(*c*), and of figure 14(*b*) with 14(*d*), shows that tension acts, as it were, to 'stretch out' the area patterns like a coiled spring.

3.3. *Shock-wave transitions*

In this paper, and in part 2, the word 'shock' connotes the experimentally observed, relatively rapid transition from a supercritical flow in a partially collapsed tube to a subcritical flow in a round, somewhat distended tube. We have never been able to produce a shock in which the downstream state was also one of partial collapse.

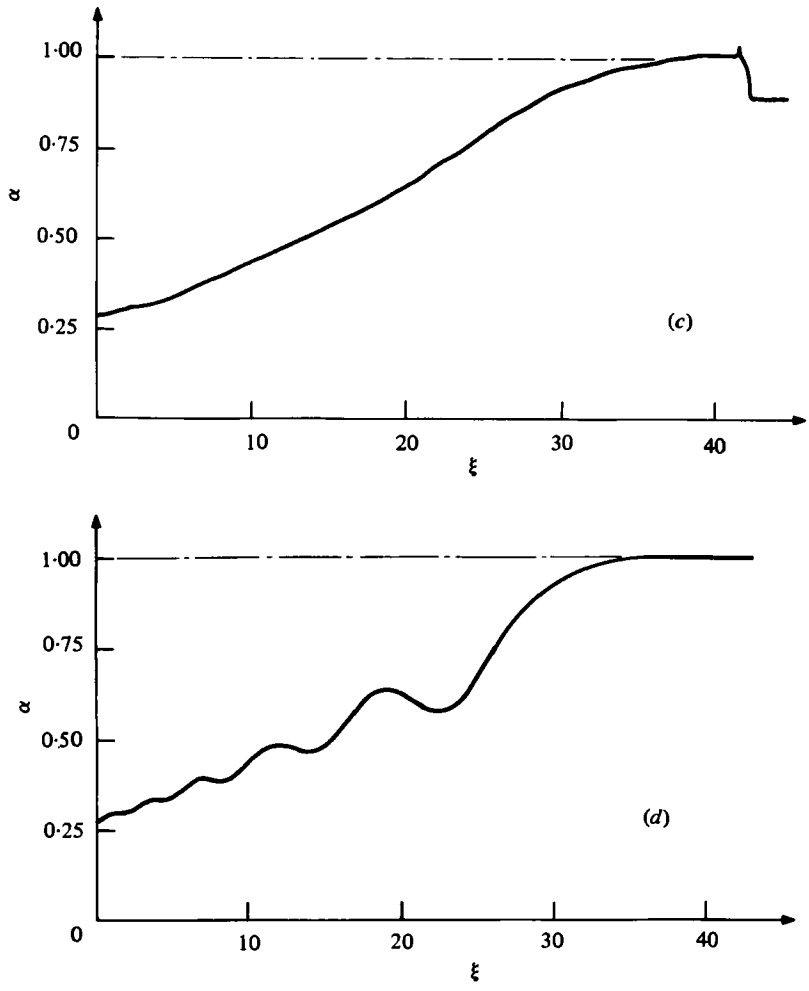

FIGURE 14. Examples of different flow patterns: (*a*) $\epsilon_x = 0{\cdot}023$, $\alpha_1 = 0{\cdot}252$, $S_1 = 1{\cdot}7$; (*b*) $\epsilon_x = 0{\cdot}023$, $\alpha_1 = 0{\cdot}270$, $S_1 = 8{\cdot}0$; (*c*) $\epsilon_x = 0{\cdot}142$, $\alpha_1 = 0{\cdot}291$, $S_1 = 6{\cdot}9$; (*d*) $\epsilon_x = 0{\cdot}174$, $\alpha_1 = 0{\cdot}290$, $S_1 = 10{\cdot}4$.

The shock region may be regarded as a diffuser whose cross-sectional shape changes in a complex manner from roughly elliptical to circular. The diffuser geometry is governed by the structural mechanics of shells and the stress loadings at the wall. The latter are intimately coupled to the mechanics of the flow, which itself depends upon the cross-sectional shapes, and which establishes the stress distribution which in part controls that shape. What is clearly a three-dimensional hydroelastic problem of great complexity is rendered even more so by the fact that the rate of area increase may involve some degree of unsteady flow separation.

It is beyond the scope of this paper, and of part 2, to deal in detail with the shock transition. We present here pressure-recovery data for the shock characterized as a diffuser. In part 2, the shock width is related to tension, area ratio and speed index by treating the forward, or supercritical, portion of the shock as the rear of the standing wave train fathered by the shock.

(*a*) *The pressure-recovery coefficient.* We employ the conventional definition

$$C_p \equiv \frac{p_2 - p_1}{\frac{1}{2}\rho u_1^2}, \tag{5}$$

where 1 refers to the location of minimum area (and thus of maximum speed u_1) at the end of the wave train preceding the shock, and 2 refers to the plateaus in area and pressure downstream of the shock.

An upper limit for C_p, applicable to a loss-free deceleration, is obtained by applying Bernoulli's equation between 1 and 2:

$$C_{p\max} = 1 - (\alpha_1/\alpha_2)^2. \tag{6}$$

For very short diffusers, a lower bound may be estimated on the assumption that there is immediate jet separation at inlet section 1, and that this is followed by a Borda–Carnot 'sudden expansion' to a larger area, with no contribution of the expanding walls to a pressure–area integral, and with negligible wall friction. Simple considerations of mass and momentum conservation, when applied to a control volume extending between sections 1 and 2, produces the result

$$C_{p\mathrm{B-C}} = 2\frac{\alpha_1}{\alpha_2}\left(1 - \frac{\alpha_1}{\alpha_2}\right). \tag{7}$$

Oates (1975) has suggested that the shock can be modelled by a similar analysis but with a pressure–area integral appearing in the momentum equation calculated on the assumption that the wall pressure is related to the area by the function $\mathscr{P}(\alpha)$ of the local tube law. This leads to

$$C_{p0} = C_{p\mathrm{B-C}} + \frac{2}{S_1^2 \alpha_1 \mathscr{P}'(\alpha_1)}\left[\frac{1}{\alpha_2}\int_1^2 \mathscr{P}(\alpha)\,d\alpha - \left(1 - \frac{\alpha_1}{\alpha_2}\right)\mathscr{P}(\alpha_1)\right]. \tag{8}$$

Owing to longitudinal tension and bending, the assumption that the local tube law relationship $\mathscr{P}(\alpha)$ prevails within the shock zone is far from correct; moreover, there are other difficulties with this model. However, such questions are rendered moot by the fact that the term in square brackets in equation (8), represented by the shaded area of figure 15, is generally very small. Because of the flatness of the function $\mathscr{P}(\alpha)$ over most of the range, the wall pressure does not rise significantly until the circular configuration has been nearly achieved. Nearly all the data shown in figure 16 are for $S_1 > 3$, and most lie in the range 5–8. In this figure, which shows $C_{p\max}$, C_{p0} and $C_{p\mathrm{B-C}}$ as functions of α_1, we have plotted C_{p0} *vs.* α_1 for the single value $S_1 = 3$. At this value the gap between C_{p0} and $C_{p\mathrm{B-C}}$ is quite small. Since the second term on the right-hand side of (8) goes as S_1^{-2}, the difference $C_{p0} - C_{p\mathrm{B-C}}$ is extremely small for most of the experiments.

(*b*) *Experimental pressure recoveries.* The measured values of C_p, which are deemed accurate to better than 10 %, are shown in figure 16 as a function of α_1. They are divided into three categories, according to the steepness of the shock: (i) 'long' diffusers, with $(1/\alpha_1)(d\alpha/d\xi)_{\max} < 0{\cdot}3$; and (ii) 'short' diffusers, with $(1/\alpha_1)(d\alpha/d\xi)_{\max} > 1{\cdot}0$; and (iii) intermediate-length diffusers, with the steepness parameter lying between 0·3 and 1·0. This crude division seems successfully to distinguish between two cases. In the 'short' diffusers, the losses are due in part to more or less severe flow separation and the dissipation subsequent thereto: the experimental values of C_p lie between $C_{p\max}$

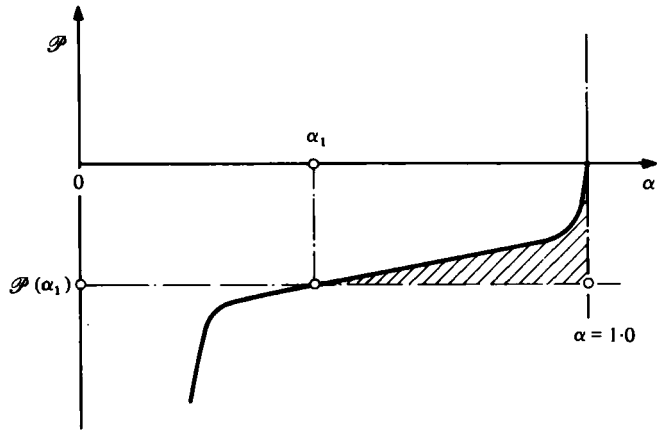

FIGURE 15. Shaded area represents the term in square brackets in equation (8).

and C_{pB-C}. In the 'long' diffusers, the flow probably does not separate, but wall friction is so large that the experimental values of C_p are even less than the Borda–Carnot values.

The intermediate-length diffusers, all of which are in a narrow range of α_1, appear to have a somewhat better pressure recovery than the short diffusers.

While not quantified, many of the experiments exhibited a certain amount of small-amplitude unsteadiness which could be observed as vibrations in the wall of the tube near the shock and which also radiated observable vibrations both upstream and downstream of the shock. This was presumably due to disturbances associated with mild flow separation and re-attachment, perhaps asymmetrically because, as remarked below, the effective angle of divergence of the diffuser was below the range where full jet separation could be expected.

(*c*) *Comparison with data for two-dimensional diffusers.* A large body of experimental information exists for two-dimensional, straight-wall diffusers (e.g. Reneau, Johnston & Kline 1967). In the literature, the pressure-recovery coefficient is correlated in terms of two geometric parameters (AR = area ratio; and N/W_1 = ratio of diffuser length to inlet width) and the dimensionless displacement thickness of the inlet boundary layer, $2\delta_1^*/W_1$. Four flow regimes, from unseparated flow to fully separated jet flow, depending upon the degree of area divergence, are generally identified.

Here we present the pressure-rise data for the shock according to a similar type of correlation. We have roughly estimated the mean inlet width as a function of α (specifically, we have taken $W_1 = 2y_1$, using the model of part 2, figure 1), and we have calculated the shock length as $N = (\alpha_2 - \alpha_1)/(d\alpha/dx)_{\max}$. The area ratio is $AR = \alpha_2/\alpha_1 = 1/\alpha_1$.

In figure 17, the pressure recovery data of figure 16 are assembled in the form of correlation employed by Reneau *et al.* The ratio $2\delta_1^*/W_1$ for our experiments is not known, but presumably it is relatively large.

According to Reneau *et al.* line A–A of figure 17 represents for two-dimensional diffusers the boundary between operation with 'no appreciable stall' and operation with 'appreciable stall'; and line B–B is the boundary between operation with 'large transitory stall' and operation with 'fully developed two-dimensional stall'. Maxi-

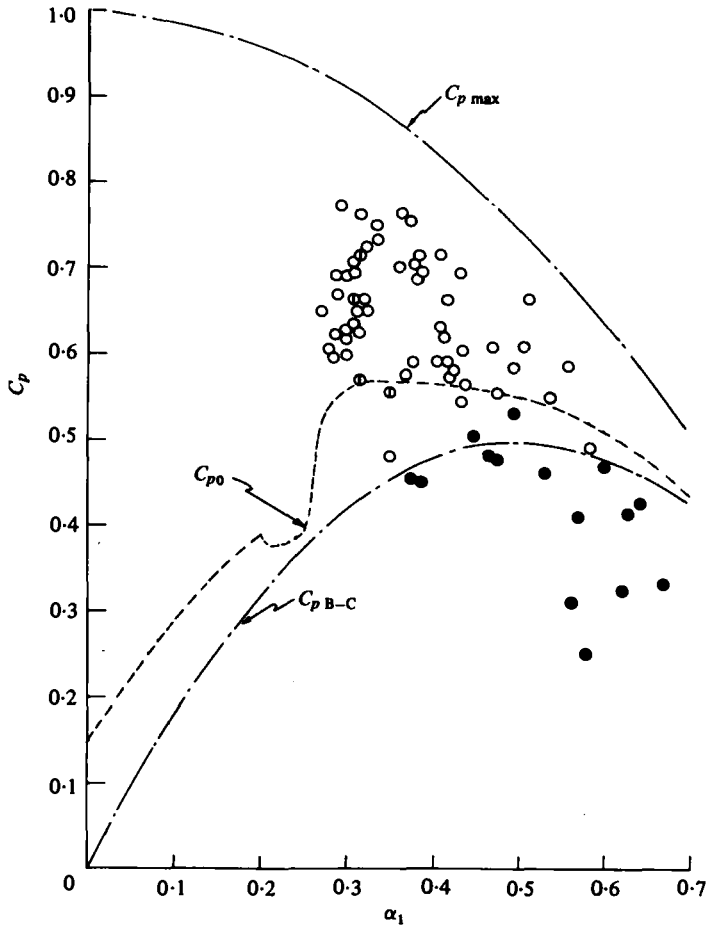

FIGURE 16. Experimental values of C_p compared with various calculated values. All the latter were based on setting $\alpha_2 = 1$, and the curve for C_{p0} is for $S_1 = 3$.

Symbol	Type	$(1/\alpha_1)\,(d\alpha/d\xi)_{max}$
●	Long	Less than 0·3
○	Intermediate	Between 0·3 and 1·0
ⓘ	Short	Greater than 1·0

mum pressure recovery for two-dimensional diffusers is achieved with operation in the neighbourhood of line A–A.

Having in mind the great differences in geometry, the experimental zones for the present data shown in figure 17 agree favourably with figures 2(*b*) and 4(*c*) of Reneau *et al.* The values of C_p are in the same range. Moreover, the curves are of similar shape and are similarly disposed with respect to line A–A.

Figure 17 appears to indicate that in the experimental shock transitions there was either 'no appreciable stall', or, if there was 'appreciable stall', it was not in the range of 'large transitory stall' and was certainly far from 'fully-developed two-dimensional stall'.

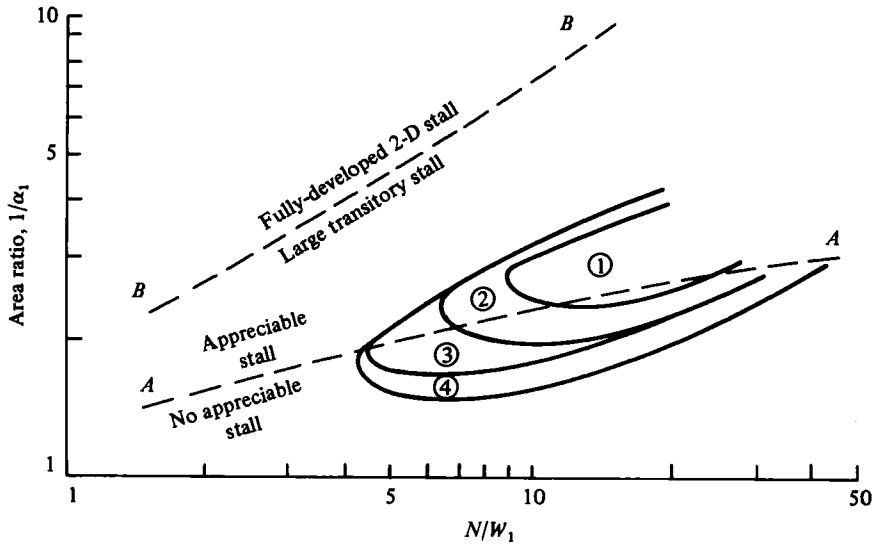

FIGURE 17. Experimental values of C_p plotted in the manner of Reneau *et al.* (1967).

Region	Maximum experimental value of C_p
1	0·77
2	0·70
3	0·60
4	0·50

Curves A–A and B–B are from figure 2 (*b*) of Reneau *et al.*

This paper and its companion paper, McClurken *et al.* (1981), are based on the theses of Kececioglu (1979) and McClurken (1980). The research was supported by the Fluid Mechanics Program of the National Science Foundation (Grant no. ENG 76-08924 and by Fellowships (to McClurken) from the National Institute for General Medical Sciences (Grants no. GM-02136 and GM-07301).

REFERENCES

ANLIKER, M., ROCKWELL, R. L. & OGDEN, E. 1971 Nonlinear analysis of flow pulses and shock waves in arteries, I, II. *Z. angew. Math. Phys.* **22**, 217–246; 563–581.

BEAM, R. M. 1968 Finite-amplitude waves in fluid-filled elastic tubes: wave distortion, shock waves, and Korotkoff sounds. *N.A.S.A. Tech. Note* TN D-4803.

ELLIOTT, E. A. & DAWSON, S. V. 1979 Fluid velocity greater than wavespeed and the transition from supercritical to subcritical flow in elastic tubes. *Med. & Biol. Engng & Comput.* **17**, 192–198.

FLAHERTY, J. E., KELLER, J. B. & RUBINOW, S. I. 1972 Post-buckling behavior of elastic tubes and rings with opposite sides in contact. *SIAM J. Appl. Math.* **23**, 446–455.

GRIFFITHS, D. J. 1969 Urethral elasticity and micturition hydrodynamics in females. *Med. & Biol. Engng* **7**, 201–215.

GRIFFITHS, D. 1971*a* Hydrodynamics of male micturition, I. Theory and steady flow through elastic-walled tubes. *Med. & Biol. Engng* **9**, 581–588.

GRIFFITHS, D. 1971*b* Steady fluid flow through veins and collapsible tubes. *Med. & Biol. Engng* **9**, 597–602.

GRIFFITHS, D. J. 1973 The mechanics of the urethra and of micturition. *Brit. J. of Urology* **45**, 497–507.

KAMM, R. D. & SHAPIRO, A. H. 1979 Unsteady flow in a collapsible tube subjected to external pressure or body forces. *J. Fluid Mech.* **95**, 1–78.

KECECIOGLU, I. 1979 Experimental determination of the structure of shock waves in fluid flow through collapsible tubes with application to the design of a flow regulator. Thesis for the Degree of Mechanical Engineer, Massachusetts Institute of Technology.

KECECIOGLU, I., KAMM, R. D. & SHAPIRO, A. H. 1978 Structure of shock waves in collapsible-tube flow. *Proc. 31st Ann. Conf. Engng Medicine & Biology, Atlanta, Georgia*, p. 92.

KIVITY, Y. & COLLINS, R. 1974 Nonlinear wave propagation in visco-elastic tubes: application to aortic rupture. *J. Biomech.* **7**, 67–76.

LAMBERT, J. W. 1958 On the nonlinearities of fluid flow in non-rigid tubes. *J. Franklin Inst.* **266**, 83–102.

MATSUZAKI, Y. & FUNG, Y. C. 1977 Stability analysis of straight and buckled two-dimensional channels conveying an incompressible flow. *J. Appl. Mech.* **44**, 548–552.

MCCLURKEN, M. E. 1978 Shape-independent area measurement in collapsible tubes by an electrical impedance technique. *Proc. 31st Ann. Conf. Engng Medicine & Biology, Atlanta, Georgia*, p. 95.

MCCLURKEN, M. E. 1980 Supercritical flow in collapsible tubes. Ph.D. thesis, Department of Mechanical Engineering, Massachusetts Institute of Technology.

MCCLURKEN, M. E., KECECIOGLU, I., KAMM, R. D. & SHAPIRO, A. H. 1981 Steady supercritical flow in collapsible tubes. Part 2. Theoretical studies. *J. Fluid Mech.* **109**, 391–415.

NICHOLSON, H. W., HEISER, W. H. & OLSEN, J. H. 1967 Wave propagation in liquid-filled elastic tubes. *Bull. Mech. Engng Education* **6**, 371–376.

OATES, G. C. 1975 Fluid flow in soft-walled tubes. Part 1. Steady flow. *Med. & Biol. Engng* **13**, 773–778.

OLSEN, J. H. & SHAPIRO, A. H. 1967 Large-amplitude unsteady flow in liquid-filled elastic tubes. *J. Fluid Mech.* **29**, 513–538.

RAMAN, K. R. 1967 Korotkoff sounds at systole: a phenomenon of dynamic instability. *J. Sci. Engng Res.* **11**, 227–268.

RENEAU, L. R., JOHNSTON, J. P. & KLINE, S. J. 1967 Performance and design of straight, two-dimensional diffusers. *Trans. A.S.M.E.* D, *J. Basic Engng* **89**, 141–148.

RUDINGER, G. 1970 Shock waves in mathematical models of the aorta. *J. Appl. Mech.* **37**, 34–37.

SHAPIRO, A. H. 1977*a* Steady flow in collapsible tubes. *Trans. A.S.M.E., J. Biomech. Engng* **99**, 126–147.

SHAPIRO, A. H. 1977*b* Physiologic and medical aspects of flow in collapsible tubes. In *Proc. 6th Canadian Cong. of Applied Mech.*, pp. 883–906.

TADBAKHSH, I. & ODEH, F. 1967 Equilibrium states of elastic rings. *J. Math. Anal. & Applics* **18**, 59–74.

WEAVER, D. S. & PAIDOUSSIS, M. P. 1977 On collapse and flutter phenomena in thin tubes conveying fluid. *J. Sound Vib.* **50**, 117–132.

WEBER, W. 1866 Theorie der durch Wasser oder andere incompressible Fluessigkeiten in elastischen Rohren fortgepflanzten Wellen. *Verh. koenigl. saechs. Ges. Wiss.* **18**, 353. Leipzig.